Construction of patient-specific computational models for organ dose estimation in radiological imaging

Tianwu Xie*, and Azadeh Akhavanallaf*
Division of Nuclear Medicine and Molecular Imaging, Geneva University Hospital, CH-1211 Geneva 4, Switzerland

Habib Zaidi[a)]
Division of Nuclear Medicine and Molecular Imaging, Geneva University Hospital, CH-1211 Geneva 4, Switzerland
Geneva University Neurocenter, Geneva University, CH-1205 Geneva, Switzerland
Department of Nuclear Medicine and Molecular Imaging, University of Groningen, University Medical Center Groningen, 9700 RB Groningen, The Netherlands
Department of Nuclear Medicine, University of Southern Denmark, 500 Odense, Denmark

(Received 13 September 2018; revised 7 February 2019; accepted for publication 8 February 2019; published 22 March 2019)

Purpose: Diagnostic imaging procedures require optimization depending on the medical task at hand, the apparatus being used, and patient physical and anatomical characteristics. The assessment of the radiation dose and associated risks plays a key role in safety and quality management for radiation protection purposes. In this work, we aim at developing a methodology for personalized organ-level dose assessment in x-ray computed tomography (CT) imaging.
Methods: Regional voxel models representing reference patient-specific computational phantoms were generated through image segmentation of CT images for four patients. The best-fitting anthropomorphic phantoms were selected from a previously developed comprehensive phantom library according to patient's anthropometric parameters, then registered to the anatomical masks (skeleton, lung, and body contour) of patients to produce a patient-specific whole-body phantom. Well-established image registration metrics including Jaccard's coefficients for each organ, organ mass, body perimeter, organ-surface distance, and effective diameter are compared between the reference patient model, registered model, and anchor phantoms. A previously validated Monte Carlo code is utilized to calculate the absorbed dose in target organs along with the effective dose delivered to patients. The calculated absorbed doses from the reference patient models are then compared with the produced personalized model, anchor phantom, and those reported by commercial dose monitoring systems.
Results: The evaluated organ-surface distance and body effective diameter metrics show a mean absolute difference between patient regional voxel models, serving as reference, and patient-specific models around 4.4% and 4.5%, respectively. Organ-level radiation doses of patient-specific models are in good agreement with those of the corresponding patient regional voxel models with a mean absolute difference of 9.1%. The mean absolute difference of organ doses for the best-fitting model extracted from the phantom library and Radimetrics™ commercial dose tracking software are 15.5% and 41.1%, respectively.
Conclusion: The results suggest that the proposed methodology improves the accuracy of organ-level dose estimation in CT, especially for extreme cases [high body mass index (BMI) and large skeleton]. Patient-specific radiation dose calculation and risk assessment can be performed using the proposed methodology for both monitoring of cumulative radiation exposure of patients and epidemiological studies. Further validation using a larger database is warranted. © *2019 American Association of Physicists in Medicine* [https://doi.org/10.1002/mp.13471]

Key words: computational models, Monte Carlo simulations, radiation dose, radiological imaging

1. INTRODUCTION

The use of x-ray computed tomography (CT) in the clinic has skyrocketed in the last decade and has been accounted as a major contributor to total radiation exposure of the population in developed countries.[1,2] As the workhorse of radiology and medical imaging, CT scans can provide fast and accurate diagnostic medical images, guide surgical interventions, and help planning therapeutic procedures.[3] Despite the overwhelming medical benefits of CT, there are concerns about potential cancer risks owing to the utilization of ionizing radiation. Overall, the radiation risks from CT imaging to patients are small as the absorbed doses commonly range from 1 to 30 mSv depending on the CT study type.[4] However, owing to the large number of CT examinations performed annually (more than 100 million worldwide),[5] even small risks may translate into a large-scaled number of future cancers. In light of these risks, accurate estimation of the absorbed dose profile and associated risk factors for the exposed patients in CT examinations is necessary.[6,7] Different

approaches have been adopted to estimate the absorbed dose to patients from CT scans, including experimental measurements using dosimeters embedded within physical anthropomorphic phantoms and Monte Carlo calculations using computational models. However, these approaches inherently bear a number of limitations including the difficulty of matching physical phantoms to the location of internal organs within the patient's body, the heavy workload involved for constructing patient-specific computational models and the inherent assumptions in measurements and simulation setups, which might contribute significant uncertainties to the estimated absorbed dose. A patient-specific phantom represents a realistic model enabling accurate estimation of organ-level dose; however, the segmentation of patient images is time consuming and not feasible for clinical routine applications. A potential alternative for person-specific organ dose estimation is to use a library of computational models where habitus-specific phantoms could serve as alternative models covering various anthropometric and anatomical characteristics of patients.[8] Several habitus-dependent phantom series have been developed to perform patient-specific dose estimation by matching anthropometric characteristics of patients, such as gender, age, height, and body weight.[9–11] Stepusin et al.[12] suggested to match patient's data to a computational phantom from a predefined library using height and weight matching for patient-specific CT dosimetry. The construction of patient-specific models from regional CT images is another alternative for patient-specific dosimetry, which was adopted in a number of studies by mapping the segmented model of patient CT images to a template anatomy through a deformable registration process.[13,14] However, this is not practical for routine clinical usage owing to the labor-intensive manual segmentation process. Kalender et al.[15] proposed to construct patient-specific whole-body models from regional CT images using a simple protocol-based appending of the scan range to a reference phantom to take out of direct field-of-view scattered radiation and overscanning effects into account. Similar to the above-mentioned method, this technique also suffers from time-consuming manual organ segmentation required for dosimetry calculations. Gao et al.[16] estimated organ doses for a large number of pediatric patients using patient-specific information implemented into VirtualDose™ CT dose calculation software. The Radimetrics™ commercial dose tracking software (Bayer HealthCare, Berlin, Germany)[17] calculates patient-specific absorbed doses by matching CT images of each patient with Cristy & Eckerman stylized computational phantoms,[18] taking into account the physical and anatomical characteristics of the patient. The ImPACT CT patient dosimetry calculator estimates organ-level absorbed doses and effective dose based on spreadsheet tools and adult stylized phantoms.[19] Although this approach is practical, it is impaired by the dosimetric uncertainties resulting from the large differences between the anatomy of patients and simulated computational phantoms (categorized by gender and age) in addition to the inherent uncertainties associated with protocol-based mapping of the scan location on the computational models.[20] Since Monte Carlo calculations using patient-specific models are commonly considered as reference for organ dose estimation from diagnostic imaging procedures,[21] the implementation of an easy to use and reliable framework enabling to estimate patient-specific organ dose for individual patients in clinical setting is highly desirable.

In this work, we propose a methodology for constructing patient-specific computational models based on deformable registration of patient CT regional images on a habitus-dependent anchor phantom. Unlike previous works that simply append the scan range to an existing reference anthropomorphic phantom, which requires labor-intensive and time-consuming manual segmentation or definition of patient's organs inside the appended region, we employ the structural deformation of the best-fitting phantom from an existing large library of computational models through automated registration to estimate the patient-specific model. We adopted three computational models for patient-specific CT dose estimation: the regional patient model developed by segmenting a series of CT images, the best-fitting/matching anchor model selected from a phantom library based on sex, age, height and weight, and patient-specific computational model constructed through image registration. Patient-specific radiation doses are calculated using the three computational models used as input to the N-Particle eXtended (MCNPX) Monte Carlo code. The results obtained using the anchor phantom and registered model are compared to the regional patient model serving as reference to investigate the influence of the computational model on the accuracy of patient-specific radiation dose estimation.

2. MATERIALS AND METHODS

2.A. Patient's regional voxel model based on CT image segmentation

The institutional ethics committee approved this retrospective study. Written informed consent was waived. CT images of four patients with different gender, age, and physical characteristics referred to Geneva University Hospital for diagnostic CT examinations were included in this work. Semiautomated image segmentation was performed using the 3DSlicer software[22] enabling to identify ten organs/tissues, including the lungs, heart wall, liver, kidneys, spleen, stomach wall, pancreas, gall bladder, urinary bladder, and skeleton. The segmented organs were validated by an experienced radiologist and integrated in a voxel matrix to produce a patient regional computational model. The chemical compositions and material density for each organ were assigned according to the ICRP report 89.[23]

2.B. Patient-specific computational phantom

In previous work, we reported on the construction of a phantom library[24] extended from ICRP reference models covering different body morphometries, consisting of about 230 male and 249 female voxel adult phantoms scaled to specific

age, height, and weight grids based on the NHANES (2011–2014) database.[25] In these series, anatomical diversity, specifically organ masses, is implemented using a multicorrelation model to estimate organ masses based on gender, age, height, weight, and BMI. Therefore, the best-fitting adult phantom is selected from the extended library to match the patient's anthropometric and anatomical characteristics. For the pediatric models, the anchor phantoms were generated by scaling the male and female ICRP adult reference phantoms to match the height and weight of actual patients. Thereafter, anatomical masks for the skeleton, lung, and body contour were generated from patients' regional CT images using autosegmentation algorithms. Subsequently, the whole-body anchor phantom is deformably registered to the patient anatomical mask model using automatic affine registration to produce a new whole-body personalized computational phantom with well-defined anatomical structures, matching patient images obtained from CT examinations. Image registration was performed using the Insight Toolkit (ITK).[26] The registration was performed in two steps: in the first step, the voxelized patient regional model was registered to the anchor phantom through automatic affine registration and the affine matrix warping the patient's regional model to the anchor phantom calculated. In the second step, the inverse affine matrix is applied to the anchor phantom to produce a new personalized computational model. The registration algorithm uses the regular step gradient descent implemented within the ITK software package and the mean squares metric between two images. The resulting model after registration is referred to as "patient-specific model" and includes 140 identified organs. Fig. 2 shows representative patient-specific computational phantoms along with the regional model of corresponding patients as well as the selected best-fitting models.

2.C. Dosimetry calculations

Computational models are commonly coupled with Monte Carlo techniques for dosimetry calculations through full simulation of the CT scanner and parameters used by the scanning protocol under which the patients were examined. The studies were acquired on the GE 750HD CT scanner (GE Healthcare, Waukesha, WI). The geometry of the system was accurately modeled and validated against experimental measurements as described in previous work.[27] The patient-specific acquisition parameters, including the table speed, revolution time, pitch factor, total collimation width, tube voltage, and modulated tube current, extracted from the DICOM headers, were modeled in this simulation setup. The examined body part was defined automatically through mapping the skeletal mask obtained from patient CT images to the whole-body computational phantoms. Obtaining the complete tube current modulation profile was not possible owing to the lack of sufficient information (proprietary data undisclosed by the manufacturer). We, therefore, extracted the longitudinal tube current modulation from the DICOM header file of patient's CT images and did not consider angular tube current modulation.[16] The absorbed doses to predefined target organs were calculated using a previously validated C++ computer code.[26,27] The simulations of each helical CT scan were repeated six times with x-ray tube starting at angles differing by 60° since the actual tube starting angles in the actual examinations were unknown. The effective dose was estimated according to ICRP report 103[28]:

$$ED = \sum_T \omega_T \sum_R \omega_R D_{R,T}, \tag{1}$$

where E is the effective dose, ω_R is the radiation weighting factor for radiation type R, $D_{R,T}$ is the contribution of radiation type R to the absorbed dose, and ω_T is the tissue weighting factor for organ or tissue T reflecting its relative radiation sensitivity.

Subsequently, clinical CT images of the patients were imported into Radimetrics™ dose tracking software[17] for calculation of organ absorbed doses and effective dose. Radimetrics™ collects CT scans directly from the hospital's picture archiving and communication system and matches patient images with Cristy & Eckerman stylized computational phantoms[18] according to age, gender, and body size. The software extracts scanning parameters (tube voltage, mAs, scan range, etc.) from the DICOM files' header information and calculates overnight patient-specific absorbed dose at the organ level through Monte Carlo simulations.

In this work, the results obtained from Monte Carlo simulations of the patient's regional model were considered as reference to which dose profiles calculated using computational models and dose monitoring software were compared.

2.D. Quantitative analysis

To investigate the impact of anatomical metrics of computational models on radiation dose estimation, habitus-dependent parameters of the computational models were compared using established metrics including the Jaccard's coefficient for each organ, organ mass, mean body perimeter, organ-surface distance, and mean body effective diameter. The similarity between the patient regional model and patient-specific model and the selected best-fitting model was evaluated through the Jaccard's coefficient:

$$J(A,B) = \frac{|A \cap B|}{|A \cup B|} = \frac{|A \cap B|}{|A| + |B| - |A \cap B|} \tag{2}$$

where $\boldsymbol{A}$ refers to the organ volume of the patient's regional model whereas $\boldsymbol{B}$ refers to the volume of the same in the patient-specific model or the selected best-fitting model. This metric enables the assessment of organs overlap between the two investigated models. The mean body perimeter was determined by the average outer perimeter of the patient in the scan range. Organ-surface distance is defined as the average distance from the skin to the organ in all slices. The body effective diameter is defined based on lateral (LAT) and anterior–posterior (AP) dimensions:

$$\textit{effective diameter} = \sqrt{AP \times LAT} \tag{3}$$

3. RESULTS

3.A. Computational models

Figure 1 shows the segmented regional model of the considered patients along with the original CT images. The best-fitting model for adult patients were selected from the extended phantom library[24] based on age, gender, and height–weight matching, while for the pediatric patients, the best-fitting models were constructed by deforming the ICRP reference model to reach the height–weight target values. The anthropomorphic characteristics of the four patients included in this study are summarized in Table I. Subsequently, the selected best-fitting model was registered to the patient's regional model to generate a patient-specific model. Figure 2 shows representative patient-specific computational models together with regional computational models of the corresponding patients and best-fitting phantoms.

The differences in terms of anthropometric metrics between the different computational models are summarized in Tables II–VI. When the results obtained using the patient's regional model serve as reference, the magnitude of the relative difference is reported based on the subtraction of the target metric from the reference value. The mean Jaccard coefficient, which describes the similarity between models, for the best-fitting models and the patient-specific models are 0.2 ± 0.17 and 0.19 ± 0.18, respectively (Table II). The absolute difference of organ mass between the actual patient and the best-fitting model ranges from -241.4% to 83.6% while the difference between the patient and the patient-specific model ranges from -251.8% to 82.2%. The mean body perimeter in the range of each organ of the patients is in the range 81.6 ± 23 cm, while the mean absolute differences for the best-fitting model and patient-specific model are 10% and 9.8%, respectively. The organ-surface distances of the patient are in the range 13.5 ± 4.1 cm for

TABLE I. Anthropomorphic characteristics of the patients and the best-fitting models (matched by gender, age, height, and weight).

Physical parameters	Patients				Best-fitting model			
	#1	#2	#3	#4	#1	#2	#3	#4
Sex	AF	AM	PM	PM	AF	AM	PM	PM
Age (yr)	50	25	7	3	40–50	20–30	–	–
Weight (kg)	88	104	26	13	89.3	105.7	26	13
Height (cm)	160	185	131	93	158.1	184.3	131	93
BMI (kg/cm^2)	34.37	30.38	15.1	15	35.77	31.22	15.1	15
Body region	Th-Ab	Th-Ab	Th-Ab	Th-Ab	WB	WB	WB	WB

AF, Adult Female; AM, Adult Male; BMI, Body Mass Index; PM, Pediatric Male; Th-Ab, Thorax-Abdomen; WB, Whole-Body.

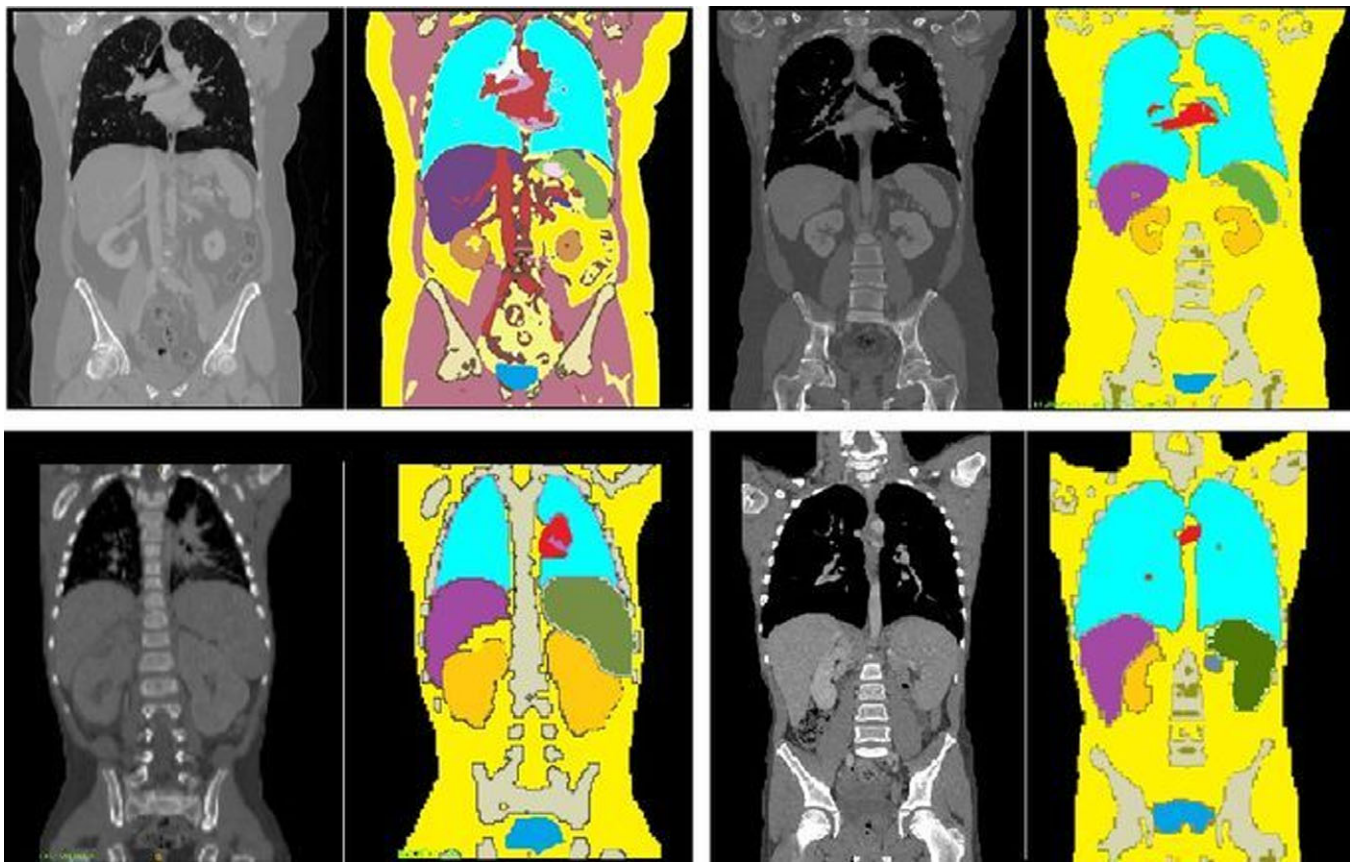

FIG. 1. Representative slices showing coronal views of segmented regional patient models for patient case #1 (top left), case #2 (top right), case #3 (bottom left), and case #4 (bottom right). [Color figure can be viewed at wileyonlinelibrary.com]

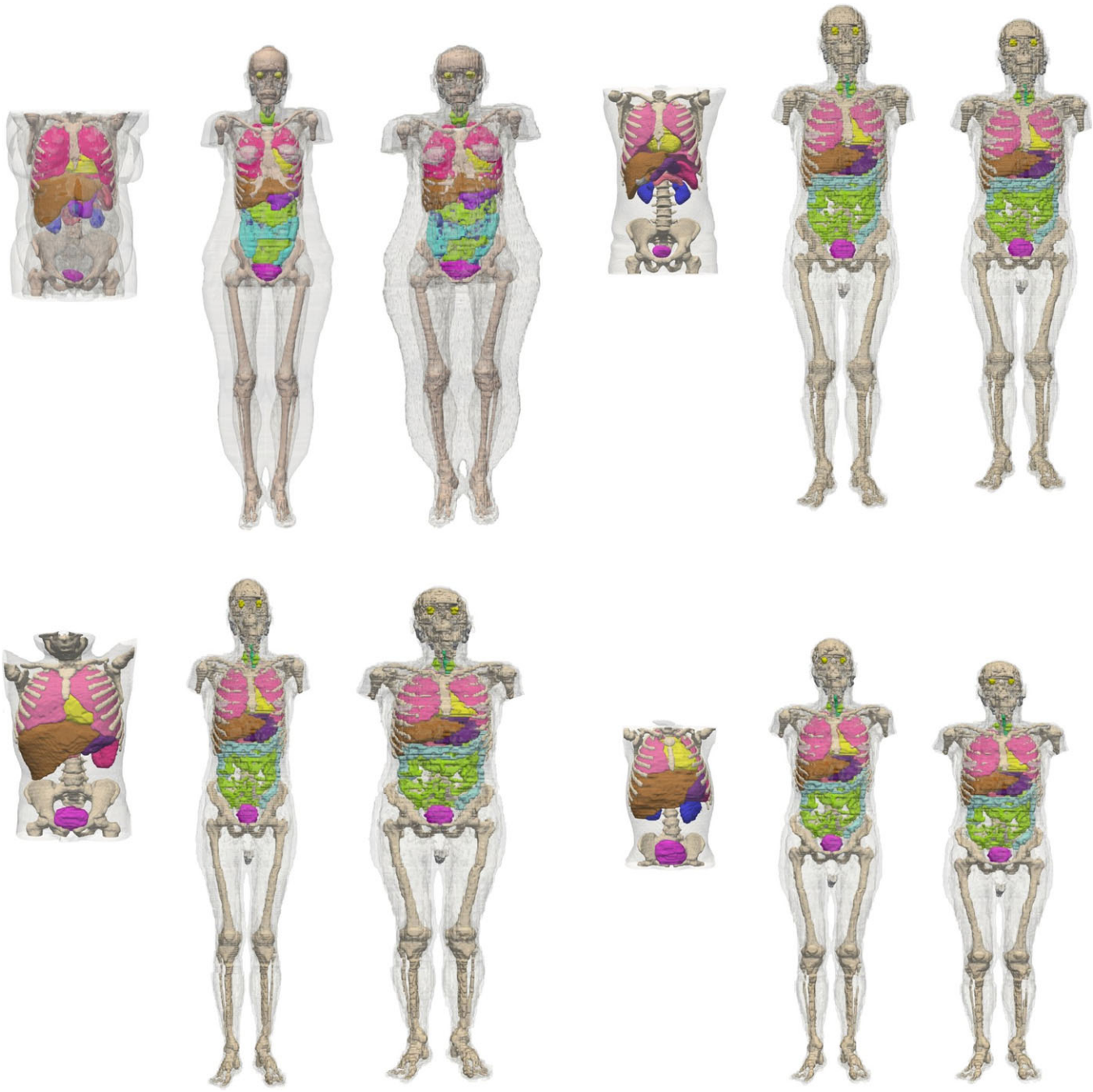

FIG. 2. Three-dimensional views of, from left to right, patients' regional models, the corresponding anchor phantoms, and patient-specific phantoms. Patient case#1 (top left), case#2 (top right), case#3 (bottom left), case#4 (bottom right). [Color figure can be viewed at wileyonlinelibrary.com]

different organs while the mean absolute difference between the best-fitting model and patient-specific model are 7.1% and 4.4%, respectively. The body effective diameters for each organ of the patient are in the range 24.6 ± 7.9 cm, while the mean absolute differences for the best-fitting model and patient-specific model are 6.6% and 4.5%, respectively.

3.B. Organ absorbed dose and effective dose

Organ radiation doses to the studied patients were calculated using the MCNPX Monte Carlo code using three computational models as input. The results were compared with the values estimated by Radimetrics™ dose monitoring software. Figure 3 shows the organ absorbed doses from CT examinations for regional computational models of patients included in this study. The mean absorbed doses to the patients are 9.2 mGy for the lung, 8.78 mGy for the heart, 10.14 mGy for the liver, 10.2 mGy for the kidney, 9.48 mGy for the stomach, 8.7 mGy for the pancreas, 9 mGy for the bladder, and 10.63 mGy for the spleen.

As shown in Figs. 4–6, when the results calculated using the patient's regional model serve as reference, the mean

absolute discordance of organ doses of the best-fitting model, the patient-specific model, and Radimetrics™ is 15.5%, 9.1%, and 41.1%, respectively. The effective dose to the patient models is 11.74, 5.96, 10.52, and 9.5 mSv for case#1, case#2, case#3, and case#4, respectively. Conversely, the values calculated using the best-fitting model, patient-specific model, and Radimetrics™ are within the range of 9.5 ± 3.3, 9.2 ± 2.14, and 10.5 ± 5.5 mSv, respectively. The absolute difference between the effective dose reported for the patient regional model and the best-fitting model, the patient-specific model, and Radimetrics™ is 15%, 5.7%, and 58.6%, respectively.

TABLE II. Jaccard's coefficients for organs between the patient regional model and other computational models.

	Jaccard Coefficients							
	Best-fitting phantom				Patient-specific phantom			
Organs	#1	#2	#3	#4	#1	#2	#3	#4
Lung	0.345	0.48	0.44	0.54	0.56	0.48	0.47	0.50
Heart	0.054	0.19	0.13	0.17	0.12	0.19	0.16	0.17
Liver	0.346	0.37	0.49	0.52	0.52	0.38	0.35	0.53
Kidney	0.287	0.15	0.15	0.22	0.21	0.16	0.14	0.19
Stomach	0.069	0.04	0.07	0.09	0.05	0.03	0.07	0.07
Pancreas	0.122	0.08	0.07	0.04	0.16	0.07	0.16	0.02
Bladder	0.016	0.04	0.0	0.04	0.01	0.04	0.09	0.05
Spleen	0.306	0.01	0.24	0.16	0.08	0.02	0.02	0.18

4. DISCUSSION

The patients' dose profiles from CT scans were calculated using different computational phantoms: the regional patient model, the best-fitting model selected using height and weight matching from previously developed phantom library, and the registered patient-specific model. When the regional patient model is used as reference, the registered patient-specific model is superior to the selected best-fitting model in terms of error in estimated organ dose. The results extracted from Radimetrics™ dose tracking software showed a considerable deviation from the reference even though the morphometric characteristics of the patient have been taken into account. Through image registration, the proposed approach allows matching the patient's data to a whole-body phantom presenting with similar location and anatomical morphometry. The evaluated metrics, including organ mass, body

TABLE III. Comparison of organ masses between the regional patient models, best-fitting, and registered models.

	Organ mass difference (%)							
	Patient vs best-fitting model				Patient vs patient-specific model			
Organs	#1	#2	#3	#4	#1	#2	#3	#4
Lungs	29.9	39.7	46.5	−44.7	−54.0	37.9	46.6	−59.5
Heart	−24.5	−22.5	0.9	31.1	−1.9	−26.2	2.1	22.5
Liver	33.1	−51.7	17.3	46.8	0.0	−55.6	17.2	41.3
Kidneys	31	−10.8	−15.3	68.6	−1.0	−14.2	−13.7	65.5
Stomach	−20.2	−188.0	−121.8	39.7	0.0	−192.2	−122.0	36.3
Pancreas	15.7	−241.4	−17.5	−225.6	2.8	−251.8	−14.3	−241.1
Bladder	−30.8	−233.3	21.5	51.1	−68.9	−242.2	20.5	44.6
Spleen	45	27.6	63.3	83.6	1.9	26.4	63.3	82.2

TABLE IV. Comparison of mean body perimeter at organ longitudinal scan range between the regional patient model and best-fitting phantom and registered models.

	Mean body perimeter difference (%)							
	Patient vs best-fitting model				Patient vs patient-specific model			
Organs	#1	#2	#3	#4	#1	#2	#3	#4
Lungs	14.4	−15.5	−12.2	−22.1	−28.8	−19.1	−26.1	−31.1
Heart	20.3	−17.3	−10.7	−20.6	−21.2	−21.2	−24.4	−29.5
Liver	22.1	−5.5	−5.4	−3.5	−17.1	−9.8	−18.7	−11.0
Kidneys	16.4	−0.9	−1.2	−1.9	−25.0	−5.2	−13.9	−9.3
Stomach	18.3	−5.5	−0.6	−1.8	−22.5	-9.9	−13.3	−9.1
Pancreas	16.3	−3.2	−0.1	2.2	−24.8	−7.8	−12.8	−5.1
Bladder	−4.3	−7.1	−9.3	−22.9	−52.7	−10.1	−23.0	−31.9
Spleen	21.4	−7.6	−5.7	−3.8	−18.0	−11.9	−19.0	−11.1

TABLE V. Comparison of organ-surface distances between the regional patient model and best-fitting phantom and registered models.

	Organ-surface distance difference (%)							
	Patient vs best-fitting model				Patient vs patient-specific model			
Organs	#1	#2	#3	#4	#1	#2	#3	#4
Lungs	19.2	−6.2	−0.5	−14.1	−5.2	−9.9	−12.8	−22.7
Heart	22.5	−7.6	−0.7	−11.8	−3.2	−11.8	−13.0	−20.2
Liver	19.9	−1.1	−1.0	0.7	−4.9	−5.0	−13.4	−6.9
Kidneys	17.4	−1.4	0.7	0.5	−8.7	−5.6	−11.3	−7.2
Stomach	16.1	−5.7	4.7	1.5	−9.9	−10.3	−7.0	−6.2
Pancreas	16.6	1.3	2.7	5.8	−9.8	−3.1	−9.2	−1.5
Bladder	−2.5	−2.4	−5.5	−13.6	−35.3	−6.6	−18.5	−22.4
Spleen	18	−3.9	−0.5	1.4	−6.3	−7.8	−12.8	−6.1

TABLE VI. Comparison of mean body effective diameters at organ longitudinal scan range between the different computational models.

	Mean body effective diameter difference (%)							
	Patient vs best-fitting model				Patient vs patient-specific model			
Organs	#1	#2	#3	#4	#1	#2	#3	#4
Lungs	20.2	−3.1	2.9	−9.7	−7.0	−7.9	−8.9	−18.1
Heart	24.7	−4.6	3.3	−10.4	−2.1	−9.4	−8.4	−18.7
Liver	18.4	1.2	0.6	0.0	−9.5	−3.4	−11.6	−7.7
Kidneys	13.7	4.5	3.0	0.7	−14.7	0.0	−8.6	−7.1
Stomach	16.5	0.8	4.2	1.7	−11.4	−3.8	−7.6	−5.8
Pancreas	12.3	2.9	3.5	3.8	−14.9	−1.6	−8.1	−264.4
Bladder	3.1	2.9	−4.6	−14.5	−29.2	−1.7	−17.3	−23.3
Spleen	19.3	0.1	0.6	0.4	−7.5	−4.5	−11.8	−7.1

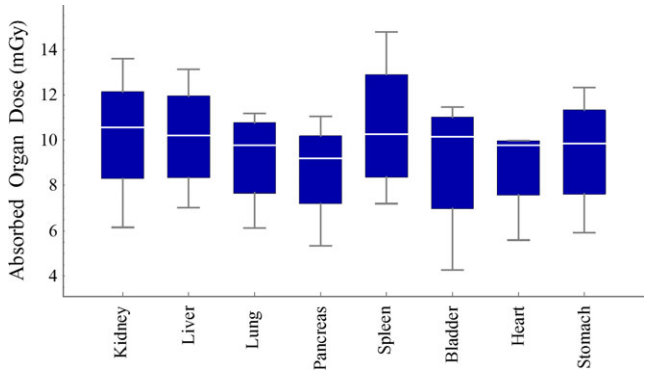

FIG. 3. Absorbed doses for segmented target organs. [Color figure can be viewed at wileyonlinelibrary.com]

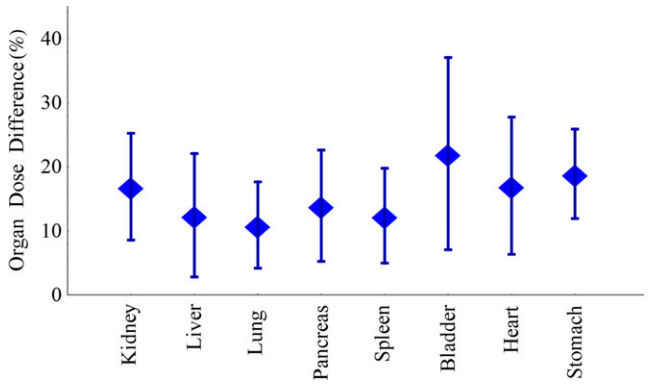

FIG. 4. Relative differences of absorbed doses in segmented target organs for best-fitting models vs patient regional models. [Color figure can be viewed at wileyonlinelibrary.com]

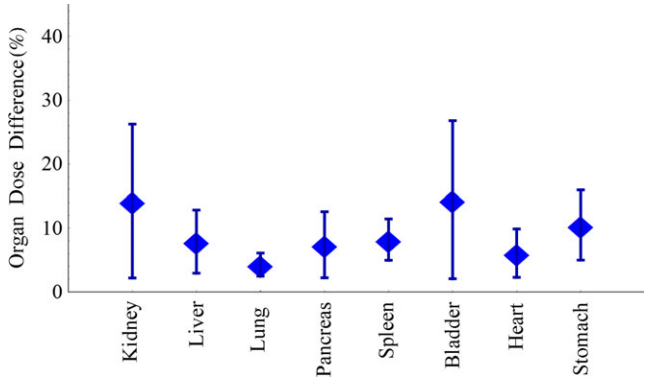

FIG. 5. Relative differences of absorbed doses in segmented target organs between patient-specific models and patient regional models. [Color figure can be viewed at wileyonlinelibrary.com]

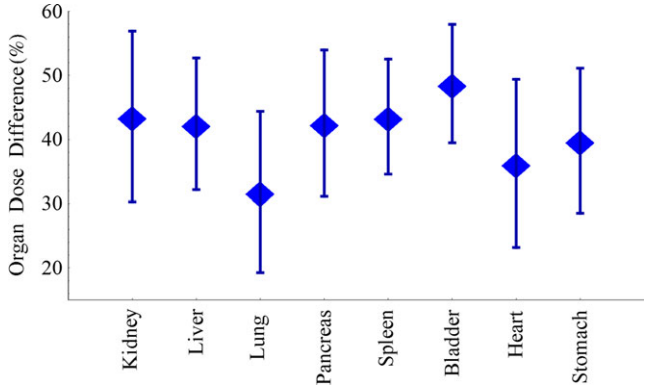

FIG. 6. Relative differences of absorbed doses in segmented target organs between Radimetrics and patient regional models. [Color figure can be viewed at wileyonlinelibrary.com]

perimeter, organ-surface distance, and effective diameter, increased in patient-specific models owing to the nonlinear deformation of the best-fitting phantom during the registration process to match the obtained anatomical masks (skeleton, lung, and body contour) of patients to the corresponding anchor phantom. The Jaccard coefficients do not show a good similarity in some cases owing to the dependency of this index on organs' volume and the spatial location of organs for the different computational models (Table II).

In this work, we selected a group of patients presenting diverse anatomical characteristics to evaluate our methodology on a representative patient population: Case #1, a patient

with high BMI and large skeleton size selected to evaluate our methodology on extreme cases and case #3, a pediatric patient presenting with a large skeleton structure. In these two cases, there is a noticeable difference in dose estimates between the reference values and the best-fitting model selected from the phantom library, even though matching patient age, height, and weight were carried out. Patient-specific models for these cases improve the dosimetric results by about 15%. Case #2 is an athletic male with small-sized internal organs whereas case #4 is a morphometrically normal pediatric patient where the best-fitting model provides organ dose estimates deviating by ~10% from the reference values without any remarkable improvement in organ dose calculation using patient-specific models.

The habitus-dependent phantom library approach suffers from the limited number of anatomies and morphometries that cause an uncertainty in dose estimation.[29] This approach provides acceptable organ doses for anthromorphically and anatomically normal patients. The current methodology building patient-specific computational models from patients' CT images demonstrated noticeable improvement in the accuracy of organ dose calculation for extreme cases. The calculated absorbed dose in the lungs is significantly improved owing to the excellent matching between the lungs mask obtained from patient CT images and the best-fitting phantom. Although Radimetrics™ dose tracking software estimates patient size from the scout scan and the examined anatomical region is determined using image registration methods, the deviation from the reference doses can be caused by the oversimplified anatomy and body contour of stylized models and the limited number of phantoms available that do not cover the diversity of different anatomies and morphometries. In addition, implementing the scan range into the simulation based on predefined CT acquisition protocols (anatomical landmarks) is another source of errors in Radimetics™.

This study bears a number of limitations, including the construction of the regional patient models for evaluation of the domestric results and the development of the phantom library. Regarding the regional patient model, the segmentation of internal organs was performed manually, where prior anatomical knowledge guides identification of organs and delimitation of their boundaries. This approach is not feasible for routine clinical application. Fortunately, the body countour, skeleton, and lungs can be automatically segmented from CT images and used during model registration to produce a patient-specific model. Likewise, assumptions regarding chemical compositions and density for organs may also introduce errors in dose estimations. Another limitation related to the selection of the best-fitting model is that the developed library contains a limited number of phantoms and cannot cover all patient morphometries. This limitation may potentially be addressed by expanding the library in future work. The limited number of patients included in this study is among the limitations of this work. In addition, the posture differences of the anchor phantom and patient studies (arms up vs arms down) may introduce a displacement of internal organs. The registration of the anchor phantom to regional patient images can be further optimized to improve the matching of the patient-specific model and patient regional model. The TCM model adopted in the simulation process did not consider the angular modulation owing to the lack of sufficient information (proprietary raw data format undisclosed by the manufacturer). Other limitations of this work include the few organs considered and the use of only one CT scanner model. The construction of patient-specific models for accurate dosimetry calculations remains a challenging issue requiring further research and development efforts.[30] Deep learning approaches have brought revolutionary advances in the field of medical image analysis that could be useful for constructing patient-specific models through automatic segmentation of medical images (body contours and internal organs).

5. CONCLUSION

The aim of this study is to quantify the dosimetric characteristics of patient-specific computational models in CT dose estimation. Although using height–weight matching to select the best-fitting model from a comprehensive phantom library is feasible in clinical setting, the estimated organ dose may differ from the reference by up to 36% as demonstrated in this study. If, however, patient CT images are available, a reference computational model can be matched to the patient data to produce a patient-specific computational model for radiation dosimetry calculations, thus improving the accuracy of organ dose estimation.

ACKNOWLEDGMENTS

This work was supported by the Swiss National Science Foundation under grant SNSF 320030_176052 and Iran's Ministry of Science and Technology.

CONFLICT OF INTEREST

The authors declare that they have no conflict of interest.

*Tianwu Xie and Azadeh Akhavanallaf contributed equally to this work
[a)]Author to whom correspondence should be addressed. Electronic mail: habib.zaidi@hcuge.ch; Telephone: +41 22 372 7258; Fax: +41 22 372 7169.

REFERENCES

1. Kalender WA. Dose in x-ray computed tomography. *Phys Med Biol*. 2014;59:R129–R150.
2. Ohno Y, Koyama H, Seki S, Kishida Y, Yoshikawa T. Radiation dose reduction techniques for chest CT: principles and clinical results. *Eur J Radiol*. 2019;111:93–103.
3. McCollough CH, Primak AN, Braun N, Kofler J, Yu L, Christner J. Strategies for reducing radiation dose in CT. *Radiol Clin North Am*. 2009;47(1):27–40.
4. Smith-Bindman R, Lipson J, Marcus R, et al. Radiation dose associated with common computed tomography examinations and the associated lifetime attributable risk of cancer. *Arch Intern Med*. 2009;169:2078–2086.

5. World Health Organization. *Communicating radiation risks in paediatric imaging: Information to support healthcare discussions about benefit and risk*. Geneva, Switzerland: World Health Organization; ISBN 978 92 4 151034 9; 2016.
6. Wang G, Crawford CR, Kalender WA. Multirow detector and cone-beam spiral/helical CT. *IEEE Trans Med Imaging*. 2000;19:817–821.
7. Cros M, Joemai RMS, Geleijns J, Molina D, Salvado M. SimDoseCT: dose reporting software based on Monte Carlo simulation for a 320 detector-row cone-beam CT scanner and ICRP computational adult phantoms. *Phys Med Biol*. 2017;62:6304–6321.
8. Moore BM, Brady SL, Mirro AE, Kaufman RA. Size-specific dose estimate (SSDE) provides a simple method to calculate organ dose for pediatric CT examinations. *Med Phys*. 2014;41:071917.
9. Xie T, Kuster N, Zaidi H. Computational hybrid anthropometric paediatric phantom library for internal radiation dosimetry. *Phys Med Biol*. 2017;62:3263–3283.
10. Johnson PB, Geyer A, Borrego D, Ficarrotta K, Johnson K, Bolch WE. The impact of anthropometric patient-phantom matching on organ dose: a hybrid phantom study for fluoroscopy guided interventions. *Med Phys*. 2011;38:1008–1017.
11. Na YH, Zhang B, Zhang J, Caracappa PF, Xu XG. Deformable adult human phantoms for radiation protection dosimetry: anthropometric data representing size distributions of adult worker populations and software algorithms. *Phys Med Biol*. 2010;55:3789–3811.
12. Stepusin EJ, Long DJ, Marshall EL, Bolch WE. Assessment of different patient-to-phantom matching criteria applied in Monte Carlo–based computed tomography dosimetry. *Med Phys*. 2017;44:5498–5508.
13. Segars WP, Sturgeon G, Li X, et al. Patient specific computerized phantoms to estimate dose in pediatric CT. *Proc SPIE Med Imaging*. 2009;7258:9.
14. Sahbaee P, Segars WP, Samei E. Patient-based estimation of organ dose for a population of 58 adult patients across 13 protocol categories. *Med Phys*. 2014;41:072104.
15. Kalender WA, Saltybaeva N, Kolditz D, Hupfer M, Beister M, Schmidt B. Generating and using patient-specific whole-body models for organ dose estimates in CT with increased accuracy: feasibility and validation. *Phys Med*. 2014;30:925–933.
16. Gao Y, Quinn B, Pandit-Taskar N, et al. Patient-specific organ and effective dose estimates in pediatric oncology computed tomography. *Phys Med*. 2018;45:146–155.
17. *Radimetrics Enterprise Platform: Dose Management Solution. Bayer HealthCare.* http://www.radiologysolutions.bayer.com/products/ct/dosemanagement/rep/.
18. Cristy M. Specific absorbed fractions of energy at various ages from internal photon sources. ak Ridge National Laboratory, Oak Ridge, TN. Report ORNL-TM-8381; 1981.
19. Wang G, Vannier MW. Helical CT image noise-analytical results. *Med Phys*. 1993;20:1635–1640.
20. Lee C, Kuzmin GA, Bae J, Yao J, Mosher E, Folio LR. Automatic mapping of CT Scan locations on computational human phantoms for organ dose estimation. *J Dig Imaging*. 2018;32:175–182.
21. Zaidi H, Ay M. Current status and new horizons in Monte Carlo simulation of X-ray CT scanners. *Med Biol Eng Comput*. 2007;45:809–817.
22. Kikinis R, Pieper S. 3D Slicer as a tool for interactive brain tumor segmentation. *Conf Proc IEEE Eng Med Biol Soc*. 2011;2011:6982–6984.
23. ICRP Publication 89. Basic anatomical and physiological data for use in radiological protection: reference values. *Ann ICRP*. 2002;32:5–265.
24. Akhavanallaf A, Xie T, Zaidi H. Development of a library of adult computational phantoms based on anthropometric indexes. *IEEE Trans Rad Plasma Med Sci*. 2019;3:65–75.
25. Vital and Health Statistics. *Anthropometric reference data for children and adults: United States, 2011–2014.* Hyattsville, Maryland: Centers for Disease Control; 2016. DHHS Publication No. 2016–1604.
26. Johnson HJ, McCormick MM, Ibanez L, and The Insight Software Consortium. *The ITK software guide*. Clifton Park, NY: Kitware; 2005. Available at https://itk.org/ItkSoftwareGuide
27. Xie T, Poletti PA, Platon A, Becker CD, Zaidi H. Assessment of CT dose to the fetus and pregnant female patient using patient-specific computational models. *Eur Radiol*. 2018;28:1054–1065.
28. ICRP publication 103: the 2007 Recommendations of the International Commission on Radiological Protection. *Ann ICRP*. 2007;37:1–332.
29. Zaidi H, Xu XG. Computational anthropomorphic models of the human anatomy: the path to realistic Monte Carlo modeling in medical imaging. *Annu Rev Biomed Eng*. 2007;9:471–500.
30. Xie T, Zanotti-Fregonara P, Edet-Sanson A, Zaidi H. Patient-specific computational model and dosimetry calculations for a patient pregnant with twins undergoing a PET/CT examination. *J Nucl Med*. 2018;59:1451–1458.